The Directional Response of Ocean Waves to Turning Winds

G. PH. VAN VLEDDER* AND L. H. HOLTHUIJSEN

Delft University of Technology, Delft, The Netherlands

(Manuscript received 23 July 1991, in final form 21 February 1992)

ABSTRACT

The directional response of ocean waves in turning wind situations has been studied with detailed wind and wave observations in open sea and with numerical simulations of the physical processes involved. The observations were acquired with pitch-and-roll buoys in the central and southern North Sea. They are selected and corrected to represent locally generated homogeneous wave fields in deep water. The response time scales thus obtained agree well with one published dataset. The disagreement with other published datasets is shown to be due to differences in analysis techniques, at least partially. The numerical simulations are carried out for homogeneous situations in which a constant wind suddenly shifts direction or rotates. These simulations show that the atmospheric input to the waves tends to rapidly turn the mean wave direction to the new wind direction. This, however, is opposed by whitecapping dissipation and nonlinear wave–wave interactions. The effect of whitecapping on the turning rate of the waves is of the same order of magnitude as that of the atmospheric input (but of opposite sign), but that of the nonlinear interactions is one order of magnitude smaller. Both observed and simulated time scales depend on the stage of development of the wave field, but the simulated time scales are considerably larger than the observed time scales.

1. Introduction

The response of waves in terms of energy and frequency to a varying wind is fairly well understood (e.g., Hasselmann et al. 1976), but our understanding of the directional response is still limited. This seems mostly due to a lack of high-quality observations and to a limited analysis of available model results. In the present study we address both aspects: we acquire and analyze a number of directional wave observations (pitch-and-roll buoys in the central and southern North Sea), and we use a numerical wave model [the third generation EXACT-NL model (Hasselmann and Hasselmann 1985)] to inspect the physical processes affecting the turning of the waves.

Buoy observations of waves turning toward the local wind direction have been presented by Hasselmann et al. (1980), who proposed a relaxation model to estimate response time scales. From their data they found that in a given sea state the time scale is shorter for the higher frequencies than for the lower frequencies. Essentially, the same results were obtained by Allender et al. (1983) and Masson (1990) using the same or similar techniques of observation and analysis. The corresponding suggestion that the response of the overall mean wave direction depends on the stage of development of the wave field was confirmed with the parametric models of Günther et al. (1981) and Holthuijsen et al. (1987). Observations of the response time scale of this overall mean direction were reported by these authors and Masson (1990). Insight in the physical processes of the turning of the waves has been provided by Young et al. (1987), who used a numerical wave model in which all relevant processes of generation and dissipation are explicitly represented (the EXACT-NL model, which was also used in the present study). They found that the initiation of the turning of the waves is mostly due to the generation of wave energy in the new wind direction. They also confirmed the tendency in the observed response time scales to be shorter with higher frequencies.

The scatter in the aforementioned observations is fairly large, possibly due to radiative effects of inhomogeneities in the wave fields. In the present study we correct our observations for such radiative effects. Moreover, we subject them to an error analysis. In addition, in our numerical simulations, we consider the role of the physical processes in more detail than in previous studies (qualitatively and quantitatively) over complete turning events.

2. Observations

a. Observation techniques and conditions

To obtain time scales of the wave directional response under turning winds we acquired wind and wave observations in the central and southern North Sea at

* Presently at Delft Hydraulics, Delft, The Netherlands.

Corresponding author address: Dr. G. Ph. van Vledder, Delft Hydraulics, P.O. Box 152, 8300 AD Emmeloord, The Netherlands.

the locations of the offshore platforms AUK-α (56°23′29″N, 02°03′56″E) and K13-α (53°13′01″N, 03°13′12″E), see Fig. 1. The depth at these locations is 70 and 30 m, respectively. The observations were taken from 25 December 1985 until 31 January 1986. The observed wind speed varied from 0.8 to 19 m s^{-1} at the K13-α location and from 1 to 27 m s^{-1} at the AUK-α location. (The maximum wind speed at AUK-α occurred at a time when no wind observations were made at the K13-α location.) The significant wave height varied from 1.0 to 7.5 m at the AUK-α location and from 0.8 to 6.5 m at the K13-α location. The wave heights at the K13-α location are generally lower than those at the AUK-α location, probably due to shallow water effects.

The anemometers were mounted at the top of the platforms at an elevation of 102 m (AUK-α) and 72.9 m (K13-α) above mean sea level. The records are 30-min averages of the observed wind speed and direction at 30-min intervals. The mean wind speed is the scalar mean; the mean direction is the vectorial mean weighted with the wind speed. The wind measurements at the K13-α platform are corrected for the effect of flow distortion caused by obstacles near the anemometer [based on wind tunnel experiments (Vermeulen et al. 1985)]. For the wind measurements at the AUK-α platform no correction for the effect of flow distortions was deemed necessary as no obstacles affected the flow near the anemometer. We converted the wind speeds to 10-m elevation (U_{10}) with a logarithmic wind profile with drag coefficient C_d given by Wu (1982):

$$C_d = (a + bU_{10}) \times 10^{-3}, \qquad (1)$$

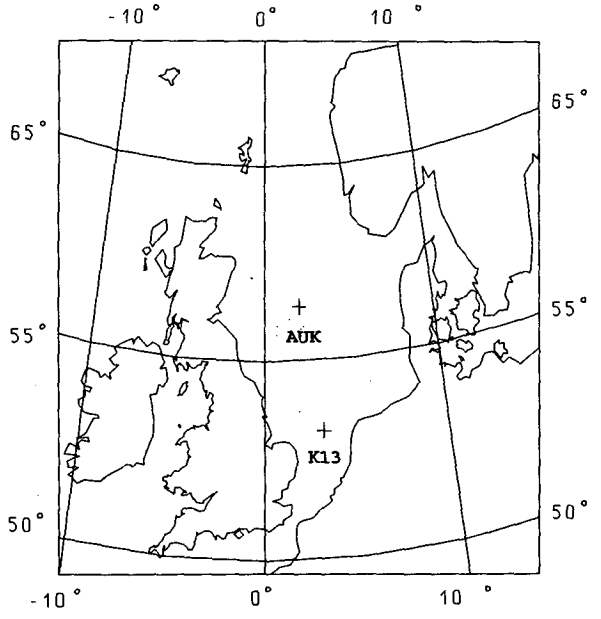

FIG. 1. Geographic locations of the observations in the central and southern North Sea.

with $a = 0.8$ and $b = 0.065$ s m^{-1}. For both locations the observed wind direction is rotated 5° counterclockwise to obtain the wind direction at 10-m elevation (to account for atmospheric boundary layer effects; e.g., Riissanen 1975).

The wave observations were obtained with WAVEC pitch-and-roll buoys (Van der Vlugt 1984) within 1-km distance from the platforms. They were analyzed with the routine analysis procedures of Kuik et al. (1988). This provided us with directional wave data at intervals of 30 min, based on 20-min time series. For the present study we consider the overall mean wave direction θ_0 (see definition below), the peak frequency f_{peak} (of the frequency spectrum), and the significant wave height H_s defined as $H_s = 4\sqrt{E_{tot}}$ (where E_{tot} is total wave variance).

b. *Analysis of the observations*

We define the time scale of the locally induced turning of the mean wave direction θ_0 toward the local wind direction θ_w in terms of the following relaxation model (see Holthuijsen et al. 1987):

$$\frac{\partial \theta_0}{\partial t} = \frac{1}{\tau} \sin(\theta_w - \theta_0) \qquad (2)$$

in which the mean wave direction θ_0 is defined as the mean direction of the wave energy:

$$\theta_0 = \arctan\left(\frac{\int_0^{2\pi} \int_0^{\infty} \sin(\theta) E(f, \theta) df d\theta}{\int_0^{2\pi} \int_0^{\infty} \cos(\theta) E(f, \theta) df d\theta} \right), \qquad (3)$$

where the wave spectrum $E(f, \theta)$ is the two-dimensional energy density as a function of frequency f and direction θ.

As the time scale τ is defined for locally induced turning, we select from the observed data with the following criteria:

1) To ensure deep-water conditions, the wave length L_{peak} associated with the observed peak frequency f_{peak} should satisfy $L_p < 3d$ (with d the local water depth).

2) To ensure actively wind-driven conditions, (i) the peak frequency f_{peak} should be higher than the direction-corrected Pierson–Moskowitz frequency ($f_{PM} = 0.13\, g/U_{10}$; Pierson–Moskowitz 1964), $f_{peak} > f_{PM}/\cos(\theta_w - \theta_0)$; (ii) the observed dimensionless wave energy ϵ ($= g^2 E_{tot}/U_{10}^4$) should be within a factor 2 from the dimensionless wave energy obtained with the $\epsilon - \nu$ relationship of Hasselmann et al. (1976), see section 3e.

3) The mean wave direction should turn toward the local wind direction.

4) To avoid unrealistic time scales in the model, the difference between the mean wave direction and the local wind direction should be less than 90°.

These criteria, however, do not ensure observations of locally induced wave turning. They are still affected to some extent by radiative effects of inhomogeneities of the wave field or by contamination with low-frequency swell. Observations that are contaminated by low-frequency swell are not rejected in this phase of the data selection. They will be dealt with after removal of the radiative effects and after the data have been selected on the basis of the results of an error analysis.

We remove the radiative effects as follows. The locally induced wave development $S(f, \theta)$ (total effect of generation and dissipation) may be written with the energy balance of the waves (e.g., Hasselmann 1960) as

$$S(f, \theta) = \frac{\partial E(f, \theta)}{\partial t} + c_g \cdot \nabla E(f, \theta), \qquad (4)$$

where the first term on the right-hand side is the local rate of change of the spectrum and the second term on the right-hand side is the radiative effect of inhomogeneities in the wave field (where c_g is the propagation velocity of the wave energy). In the present study we correspondingly estimate the locally induced development of the mean wave direction θ_0 (due to the source term S) from observed local rates of change of θ_0 and from hindcasted radiative effects. To that end the energy balance of Eq. (4) is expressed in terms of the cosine and sine of the mean wave direction θ_0 (a and b, respectively) as follows:

$$\begin{pmatrix} \partial a/\partial t \\ \partial b/\partial t \end{pmatrix}_S = \begin{pmatrix} \partial a/\partial t \\ \partial b/\partial t \end{pmatrix}_{\text{observed}} + \begin{pmatrix} \partial a/\partial t \\ \partial b/\partial t \end{pmatrix}_{\text{hindcasted}}. \qquad (5)$$

Application of the definition operator of θ_0 to the energy balance equation shows that the hindcasted radiative effect is (see also Appendix)

$$\begin{pmatrix} \partial a/\partial t \\ \partial b/\partial t \end{pmatrix}_{\text{hindcasted}} = \int_0^{2\pi} \int_0^{\infty} \begin{pmatrix} \cos(\theta) \\ \sin(\theta) \end{pmatrix} \{ c_g \cdot \nabla E(f, \theta) \} \, df d\theta. \qquad (6)$$

The value of $c_g \cdot \nabla E(f, \theta)$ is determined from hindcasts with the numerical wave model WINCH of Oceanweather, Inc., at the Norwegian Meteorological Institute in Oslo (Greenwood et al. 1985; Eide et al. 1986), driven by 2-h wind fields of the U.K. Meteorological Office fine-mesh model (both models 1985 status).

The time series of the cosine and sine of locally induced θ_0 (indicated with *) are subsequently obtained with (see Appendix)

$$\begin{pmatrix} a \\ b \end{pmatrix}^*_{j+1} = \begin{pmatrix} a \\ b \end{pmatrix}_{j+1,\text{observed}} + (2\Delta t) \begin{pmatrix} \partial a/\partial t \\ \partial b/\partial t \end{pmatrix}_{j,\text{hindcasted}}, \qquad (7)$$

where Δt is the observation interval and j is a discrete time-step indicator. The technique used to estimate the response time scale from these time series is based on a finite-difference version of the relaxation model:

$$\tau(t_j) = \frac{t_{j+1} - t_{j-1}}{\theta^*_{0,j+1} - \theta_{0,j-1}} \sin(\theta_{w,j} - \theta_{0,j}). \qquad (8)$$

This procedure of removing the radiative effect adds errors of the hindcast to the errors in the observation of τ. To evaluate the effects of both these errors, we carry out an error analysis based on a conventional first-order error propagation technique, after which the corrected time-scale estimates are finally selected on the basis of their relative error. Consider the time scale τ as a function Φ of the above variables represented by ξ_i. For statistically independent variables, the error of τ (standard deviation σ_τ) is then given by (e.g., Mood et al. 1974)

$$\sigma_\tau^2 = \sum_{i=1}^{N} \left(\frac{\partial \Phi}{\partial \xi_i} \right)^2 \sigma_{\xi_i}^2, \qquad (9)$$

in which σ_τ and σ_{ξ_i} are the standard deviations of the estimate of τ and the independent variables ξ_i, respectively. In the analysis we assume that the total wave energy propagates with the deep-water propagation speed of the hindcasted peak frequency f_M in the hindcasted mean wave direction θ_M. In that case the independent variables are (dropping the time index) θ_0, θ_w, and E_{tot}, in the observations. They have been chosen as follows: $\sigma_{\theta_0} = 4°$, $\sigma_{\theta_w} = 8°$, and $\sigma_{E_{\text{tot}}} = 0.1\, E_{\text{tot}}$. The standard deviations for the model parameters θ_M and f_M are computed as the standard deviation of the error in the actual hindcasts over all observations considered (errors obtained from comparisons with the WAVEC buoys). The values of $\partial E_{\text{tot}}/\partial x$ and $\partial E_{\text{tot}}/\partial y$ can be estimated from finite differences in the model results. But the errors in the corresponding computed values of E_{tot} at neighboring grid points are highly correlated. The apparent errors in $\partial E_{\text{tot}}/\partial x$ and $\partial E_{\text{tot}}/\partial y$ are consequently small, and we ignore them in the error analysis. [Details of the error analysis can be found in Van Vledder (1990).]

After selecting the observations with the above criteria of acceptable geophysical conditions, we correct the remaining data for the radiative effects and determine the error σ_τ for each observation as indicated above. We subsequently normalize the time scale with the friction velocity $u_*^2 = C_d U_{10}^2$ [*with* C_d from Eq. (1)] and the gravitational acceleration g to obtain τ_* ($=g\tau/u_*$). In addition, we have quantified the effect of the correction by computing the difference between the corrected and uncorrected time-scale estimates ($\Delta\tau_* = |\tau_*^{\text{corrected}} - \tau_*^{\text{uncorrected}}|$).

c. *Results of the observations*

The observed time series contain 1261 time intervals of 1 hour [two intervals of 30 min being required for one estimate of τ, see Eq. (8)]. Each interval contains

TABLE 1. Percentage of time intervals rejected for the time-scale analysis by different selection criteria if applied separately and simultaneously.

Criterion	Percentage rejected (%)
Deep water	40
$\lvert\theta_w - \theta_0\rvert < 90°$	7
Waves turn toward wind direction	65
$\epsilon - \nu$ relationship	40
All criteria simultaneous	89

three wave observations, three wind observations, and one wave model result. The selection described reduces this number to 133 accepted time intervals (11% of the original data). The effects of the various criteria are summarized in Table 1.

The results are shown in Fig. 2a as a function of wave age for which we use the dimensionless peak frequency ν_*, defined as $\nu_* = f_{\text{peak}} u_*/g$. The considerable scatter in these results is obvious. Filtering the data by limiting the allowable relative error σ_τ/τ reduces the scatter but of course also the number of data points, as shown in Fig. 2b, c, d and Table 2. The observations in Fig. 2 show that the decrease in scatter exposes an increasing correlation with an obvious trend of smaller time scales for younger sea states. To each of these four sets of observed time-scale estimates, a linear least-squares fit of $\log(\tau_*) = \log(a) + b \log(\nu_*)$ has been applied. For each set the coefficient of linear correlation has been computed, as well as the estimated standard deviation in the regression coefficients; see Table 2. The results of the regression analysis indicate an increasing correlation as the relative error is reduced, except for the case where $\sigma_\tau/\tau < 0.5$. From a subjective assessment of the standard deviations, the number of

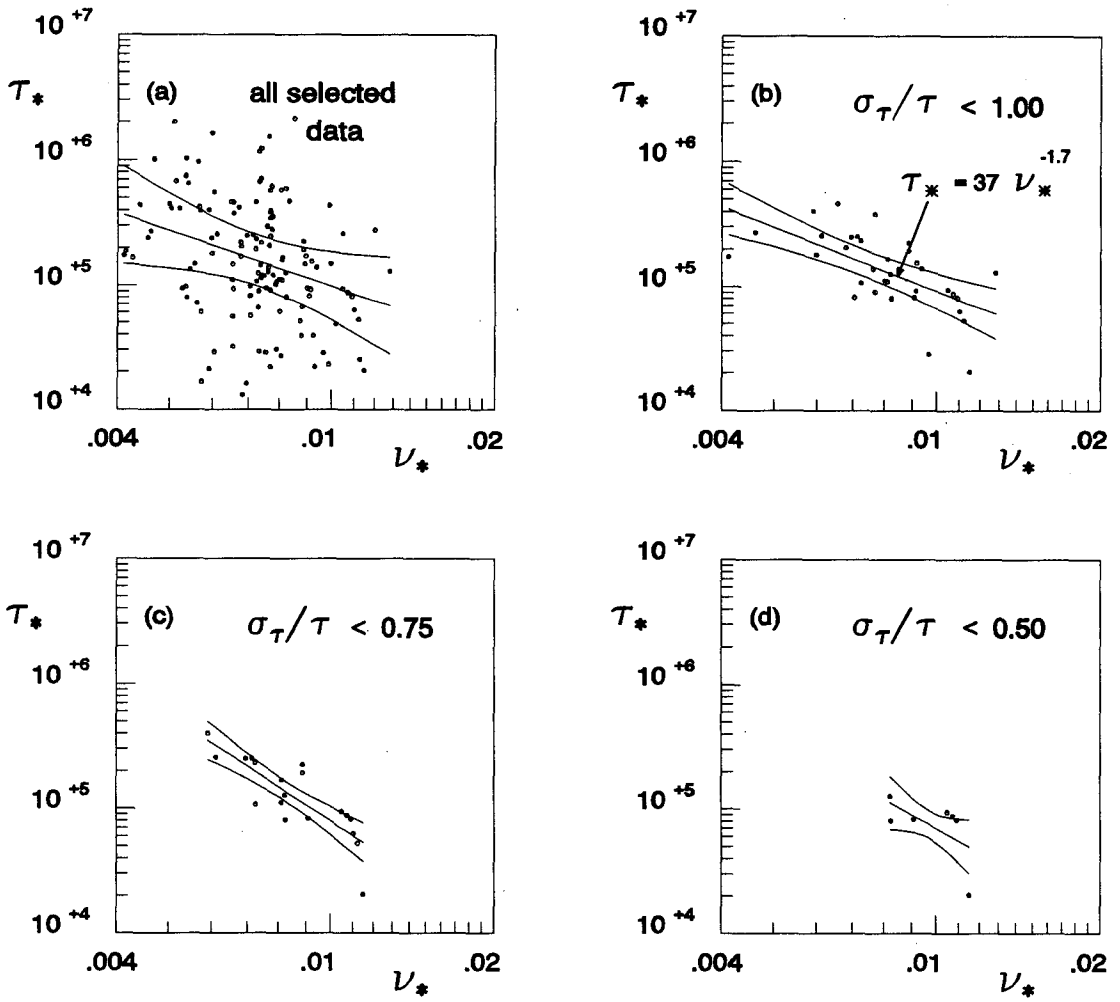

FIG. 2. Dimensionless response time scale (τ_*) of the mean wave direction turning toward the local wind direction as a function of wave age (ν_*), as observed in the present study. The effect of filtering the observations with the acceptable relative error (σ_τ/τ) is shown. The best-fit line through the data and the 95% confidence intervals of the best-fit line are indicated.

TABLE 2. Remaining number of observations and results of best-fit analysis as a function of relative error in observed response time scale. Shown are the coefficients of linear correlation between $\log(\nu_*)$ and $\log(\tau_*)$ with their 95% confidence intervals, the estimated values and the standard deviation of the regression coefficients $\log a$ and b, and the estimated value of a.

Relative error σ_τ/τ less than	Number of observations	Correlation coefficient	$\log a \pm$ std. dev	$b \pm$ std. dev	a
∞ (all selected data)	133	−.31 (−.46, −.15)	2.05 ± 0.85	−1.4 ± 0.4	112
1.00	34	−.62 (−.79, −.35)	1.57 ± 0.80	−1.7 ± 0.4	37
0.75	19	−.82 (−.93, −.59)	−0.79 ± 0.98	−2.8 ± 0.5	0.16
0.50	7	−.57 (−.93, +.32)	0.01 ± 1.56	−2.4 ± 1.6	1.0

remaining data points, and the range of wave age, we deem the results for $\sigma_\tau/\tau < 1.00$ as the most representative:

$$\tau_* = 37\nu_*^{-1.7}. \quad (10)$$

Although the application of criterion 2 removes swell-dominated cases, all of the selected 133 spectra have been inspected for a possible contamination with low-frequency swell. Only six of these spectra contained a minor low-frequency peak (frequency lower than peak frequency).

By repeating the analysis without the hindcast corrections, it was found that this has a negligible effect on the position of the best-fit line [Eq. (10)]. The correlation between $\log(\nu_*)$ and $\log(\tau_*)$, however, decreases by about 5%, and the relative change of each time scale due to the correction has an average of about 25% (positive or negative). In addition, the sum of the squared differences increases by about 25%. The hindcast-related error in τ_* is generally less than half the correction of τ_*.

d. Comparison with published observations

Günther et al. (1981), Holthuijsen et al. (1987), and Masson (1990) observed changing wave directions at sea with a buoy and estimated the response time scale of the (frequency independent) overall mean wave direction. Holthuijsen et al. (1987) defined θ_0 as in Eq. (3), whereas Günther et al. (1981) and Masson (1990) defined the mean wave direction as the mean direction of wave momentum (somewhat biased toward the higher frequencies compared with θ_0). The observed time scales have been expressed in terms of a coefficient χ due to Günther et al. (1981), who parameterized the energy balance of the waves to obtain

$$\tilde{\tau} = \chi^{-1}\nu^{-2}, \quad (11)$$

where the dimensionless time scale is $\tilde{\tau} = g\tau/U_{10}$ and the dimensionless peak frequency is $\nu = f_{\text{peak}}U_{10}/g$. For a given situation, the observed values of τ, f_{peak}, and U_{10} can thus be transformed to an estimate of the coefficient χ. The mean values of χ of Günther et al. (1981), Holthuijsen et al. (1987), and Masson (1990) are given in Table 3. The corresponding relationships in terms of τ_* and ν_* are obtained with $C_d = 0.001736$ [the average value for C_d of Eq. (1) for wind speeds of 10 and 20 m s^{-1}]. They are given in Fig. 3a (within the range of observations of wave age; see Table 3). For our data the average χ value is 0.57×10^{-2} [see Table 3; χ value obtained from each $\tilde{\tau}$ value using Eq. (11) for $\sigma_\tau/\tau < 1.0$], but the best-fit through our data (i.e., the 34 selected time-scale estimates with $\sigma_\tau/\tau < 1.0$) supports a power of ν_* [in Eq. (11)] somewhat less than 2 [Eq. (10)].

Instead of observing the response time scale of the overall mean wave direction, Hasselmann et al. (1980) observed the response time scale of the mean wave direction at each frequency $\theta_{0,f}$ turning toward the wind direction θ_w. This frequency-dependent mean wave direction $\theta_{0,f}$ is defined as (Longuet-Higgins et al. 1963)

TABLE 3. Values of the time-scale coefficients b and χ and fit ranges from various sources (observations; computations with the EXACT-NL model).

Source	χ value (rad)	b value: original	b value: reanalyzed	Interval in ν_* space	Number of τ_* estimates
Günther et al. (1981)	0.21×10^{-2}	—	—	0.007–0.012	4
Holthuijsen et al. (1987)	0.41×10^{-2}	—	—	0.054–0.02	8
Masson (1990)	0.12×10^{-2}	3.1×10^{-5}	—	0.0066–0.0132	45
Hasselmann et al. (1980)	—	2.0×10^{-5}	6.0×10^{-5}	0.0066–0.0132	42
Allender et al. (1983)	—	1.7×10^{-5}	12.1×10^{-5}	0.0073–0.0119	27
Young et al. (1987, EXACT-NL model)	—	10.0×10^{-5}	—	0.011–0.017	—
This study (observations, $\sigma_\tau/\tau < 1.0$)	0.57×10^{-2}	—	—	0.004–0.0128	34
This study (EXACT-NL model)	0.16×10^{-2}	—	—	0.007–0.011	113

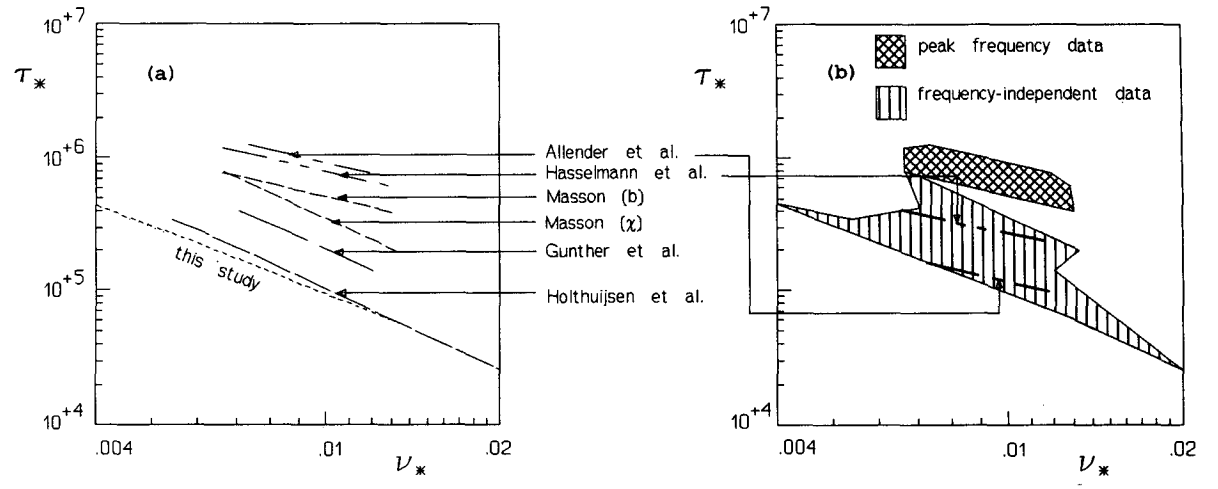

FIG. 3. Dimensionless response time scale (τ_*) as a function of wave age (ν_*), as reported in the literature and partly reinterpreted, panel (a). The regression line of the observations in the present study (Fig. 2b) is shown. The clustering of the data in two families is indicated with the two fill patterns of the envelopes of the two families, panel (b). The data of Hasselmann et al. (1980) and Allender et al. (1983) shift to lower values of τ_* after our reanalysis, panel (b).

$$\theta_{0,f} = \arctan\left(\frac{\int_0^{2\pi} \sin(\theta)E(f,\theta)d\theta}{\int_0^{2\pi} \cos(\theta)E(f,\theta)d\theta}\right). \quad (12)$$

The corresponding frequency-dependent time scale τ_f is defined in terms of a frequency-dependent relaxation model,

$$\frac{\partial\theta_{0,f}}{\partial t} = \frac{1}{\tau_f}\sin(\theta_w - \theta_{0,f}). \quad (12)$$

In their analysis Hasselmann et al. (1980) assume the time scale to be dependent on frequency as $\tau_f = (2\pi bf)^{-1}$. They estimated b values with a one parameter regression technique correlating the observed rate of turning $\partial\theta_0/\partial t$ with $2\pi f \sin(\theta_w - \theta_0)$. Allender et al. (1983) and Masson (1990) performed an identical analysis of their observations with similar results. The average b values from these studies are summarized in Table 3 (labeled "original").

To compare the frequency-independent time scale τ (expressed in terms of the χ value) with the frequency-dependent time scale τ_f (expressed in terms of the b value), we assume that the directional response of the waves is dominated by the peak frequency. This assumption seems to be reasonable for the fairly narrow spectra of actively growing wind seas. We consequently apply the frequency-dependent expressions of Hasselmann et al. (1980), Allender et al. (1983), and Masson (1990) to the peak frequency. For the subsequent transformation to the dimensionless time scale (τ_*) and wave age (ν_*), we use the same value for C_d as before ($C_d = 0.001736$). The result is shown in Fig. 3a, where it is obvious that the observations separate into two families: the original frequency-dependent data, as applied to the peak frequency, on the one hand, and the frequency-independent data on the other (Fig. 3b). The discrepancies between the two families may well be due to the transformation of the frequency-dependent observation, to a difference in estimation procedures, or to a difference in the selection of the observations. In the estimation procedures one essential difference seems to be that in the analysis of the frequency-independent observations each b value is determined from one individually observed rate of turning [with the finite-difference technique of Eq. (8)] and then averaged, whereas in the frequency-dependent analysis the rates of turning are first clustered (per class of U_{10}/c) to obtain one b value per class (using the one parameter regression technique). These were then averaged over the classes.

To investigate this potential source of discrepancy we reanalyzed the published time series of Hasselmann et al. (1980) and Allender et al. (1983) with both our finite-difference technique and their regression technique. In the finite-difference method, we determined the b value per time step, grouped the results in the classes of U_{10}/c as used by these authors, and determined the unweighted average. The results of our reanalysis for the data of Allender et al. (1983; their Figs. 3, 4, and 5, containing all their data) is an average value of b that is a factor 8 larger than the original value (see Table 3). The same analysis is applied to the illustrations of Hasselmann et al. (1980), which unfortunately contain only 37% of all their data. The average value of b thus obtained is a factor 3 larger than the original value (see Table 3). These differences are appreciable, and they bring the data of Hasselmann et al. (1980) and Allender et al. (1983) within the range of Günther et al. (1981) and Holthuijsen et al. (1987),

as shown in Fig. 3b. In the regression method, we determined the $\partial\theta_0/\partial t$ and $2\pi f \sin(\theta_w - \theta_0)$ values per time step, grouped the results in the previously used classes, performed a one parameter regression analysis per class to obtain an estimate of b, and determined the unweighted average. The results of the reanalysis are summarized in Table 4.

To determine the effect of different selection criteria, we subjected the data of Hasselmann et al. (1981) and Allender et al. (1983) to the criteria of Holthuijsen et al. (1987; not all of our criteria could be used due to lack of information):

- wave direction turns toward the wind direction;
- maximum directional difference with the wind direction 90°;
- the minimum difference between mean wave direction and wind direction should be 10°; and
- the mean wave direction changes at least 10° between two consecutive observations.

The effects of these selection criteria on the results are shown in Table 4. This selection is rather severe as it removed 140 of the 167 observations of Allender et al. (1983), and 138 from the 180 observations of Hasselmann et al. (1980). For our finite-difference technique, the effect of this selection on the average value of b in these sets is marginal: less than 5% in both cases. For the regression technique, however, this effect increases the average value of b by as much as 30%.

The results shown in Table 4 also indicate that the regression technique produces lower b values than our finite-difference method. The large reduction of remaining data of Hasselmann et al. (1980) shows that Hasselmann et al. (1980) used other criteria in choosing their illustration than the foregoing criteria.

It is obvious from Fig. 3 that our observations agree well with those of Holthuijsen et al. (1987) and the reanalyzed data of Allender et al. (1983).

3. The numerical simulations

a. *The wave model*

To investigate the physical processes affecting the turning of waves (excluding propagation effects), we use the numerical wave model EXACT-NL (Hasselmann and Hasselmann 1985). It is a one-dimensional, deep-water model in the sense that fetch-limited or duration-limited cases can be considered. We consider the duration-limited case (i.e., homogeneous situations) in which the time evolution of the wave field is controlled by the source terms only:

$$\frac{\partial E(f,\theta)}{\partial t} = S_{in}(f,\theta) + S_{ds}(f,\theta) + S_{nl}(f,\theta), \quad (14)$$

where $S_{in}(f,\theta)$, $S_{ds}(f,\theta)$, and $S_{nl}(f,\theta)$ are the two-dimensional source functions for atmospheric (wind) input, whitecapping, and nonlinear wave–wave interactions, respectively. For S_{in}, the expression of Snyder et al. (1981), modified by Komen et al. (1984), is used:

$$S_{in}(f,\theta) = \max\left[0,\ 0.25\,\frac{\rho_a}{\rho_w}\,\omega\left\{28\left(\frac{u_*}{c}\right)\times\cos(\theta-\theta_w)-1\right\}E(f,\theta)\right], \quad (15)$$

where ρ_a is the density of air, ρ_w the density of water, $\omega = 2\pi f$ is the radian frequency, c is the phase velocity of a wave component with frequency f, and θ_w is the wind direction. For the whitecapping dissipation, the expression proposed by Komen et al. (1984) is used:

$$S_{ds}(f,\theta) = -C\bar{\omega}\left(\frac{\omega}{\bar{\omega}}\right)^n\left(\frac{\hat{\alpha}}{\hat{\alpha}_{PM}}\right)^m E(f,\theta), \quad (16)$$

in which $C = 3.33 \times 10^{-5}$, $m = 2$, $n = 2$, $\bar{\omega} = 2\pi \iint f E(f,\theta)\,df\,d\theta/E_{tot}$, $\hat{\alpha}$ is the squared wave steepness $\hat{\alpha} = E_{tot}\bar{\omega}^4/g^2$, and $\hat{\alpha}_{PM} = 4.57 \times 10^{-3}$ is the value of $\hat{\alpha}$ for a Pierson–Moskowitz spectrum (Pierson and Moskowitz 1964). The nonlinear wave–wave interactions are from Hasselmann (1962):

$$S_{nl}(\mathbf{k}_4) = \int_{-\infty}^{+\infty}\int_{-\infty}^{+\infty}\int_{-\infty}^{+\infty} \omega_4 G(\mathbf{k}_1,\mathbf{k}_2,\mathbf{k}_3,\mathbf{k}_4) \times \delta(\mathbf{k}_1+\mathbf{k}_2-\mathbf{k}_3-\mathbf{k}_4)\delta(\omega_1+\omega_2-\omega_3-\omega_4) \times [N_1N_2(N_3+N_4)-N_3N_4(N_1+N_2)] \times d\mathbf{k}_1 d\mathbf{k}_2 d\mathbf{k}_3, \quad (17)$$

in which G is the coupling coefficient given by

$$G = \frac{\pi g^2 D^2}{4\rho_w^2\omega_1\omega_2\omega_3\omega_4} \quad (18)$$

and $N_i = N(\mathbf{k}_i)$ is the action density at wave number $\mathbf{k}_i$, and D is an interaction coefficient that is a com-

TABLE 4. Comparison of the original and reanalyzed values of the relaxation coefficient b of the published data of Allender et al. (1983) and Hasselmann et al. (1980), based on a finite-difference method and a one-parameter regression technique, and by applying the selection criteria of section 2d. The number of remaining estimates is shown in brackets.

		Regression analysis		Finite differences		
	Original b	No selection b	Selection b	No selection b	Selection b	Number of estimates
Allender et al. (1983)	2.0×10^{-5}	8.1×10^{-5}	10.9×10^{-5}	11.7×10^{-5}	12.1×10^{-4}	167 (27)
Hasselmann et al. (1980)	1.7×10^{-5}	3.4×10^{-5}	4.5×10^{-5}	5.7×10^{-5}	6.0×10^{-5}	180 (42)

plicated function of the four wave numbers involved in each interaction. In the EXACT-NL model these nonlinear interactions are computed with the method of Hasselmann and Hasselmann (1981).

We use a frequency resolution of $\Delta f = 0.1f$ in the frequency range 0.070–0.918 Hz for the cases with wind speed $U_{10} = 10$ m s^{-1} ($u_* = 0.381$ m s^{-1}), and a frequency resolution of $\Delta f = 0.12f$ in the frequency range 0.030–0.640 Hz for the cases with wind speed $U_{10} = 20$ m s^{-1} ($u_* = 0.917$ m s^{-1}). The directional resolution $\Delta\theta = 30°$ over the full circle.

b. *Simulation conditions*

The evolution of the wave field is considered in two turning wind situations. In the first situation a constant wind ($U_{10} = 10$ and 20 m s^{-1}) generates a homogeneous wave field until the peak frequency has decreased to twice the Pierson–Moskowitz peak frequency. The wind then suddenly shifts direction and remains constant again. We consider four directional shifts: 30°, 45°, 60°, and 90°. In the second turning wind situation the wind ($U_{10} = 10$ m s^{-1}) is not shifted to a new constant direction, but it starts to rotate after the waves have reached twice the Pierson–Moskowitz peak frequency (at a constant rate $\Omega = 10°$ h^{-1}). The computations are carried out until a stationary situation is reached. In the constant-wind cases this situation is considered to be reached when the mean wave direction is within 1° from the new wind direction, and in the rotating wind case when the lag $\delta\theta$ between mean wave direction and wind direction is constant within 1°.

c. *Analysis of the model results*

We quantify the time scale τ of the overall mean wave direction with the frequency independent relaxation model of Eq. (2). For the sudden wind shift the analytical solution of this model with a constant τ would be (Young et al. 1987)

$$-\ln\left[\frac{\tan\{\frac{1}{2}(\theta_w - \theta_0)\}}{\tan\{\frac{1}{2}\theta_w\}}\right] = \frac{t}{\tau}. \qquad (19)$$

The left-hand side of this equation would then be proportional to time t. Considering the EXACT-NL model results (Fig. 4), however, it is obvious that τ is not a constant. In fact, the time scale is usually considered to be a function of wave age (see Introduction) that changes during the wave response (Fig. 6d). We therefore estimate the value of τ as a function of time from the model time series of θ_0 with the same finite-difference scheme as we used in the analysis of our observations, except that now the time intervals in the finite-difference scheme are those of the model results. (See next section.)

The time series of θ_0 computed with the EXACT-NL model contain some high-frequency numerical noise that spuriously affects the estimated values of τ.

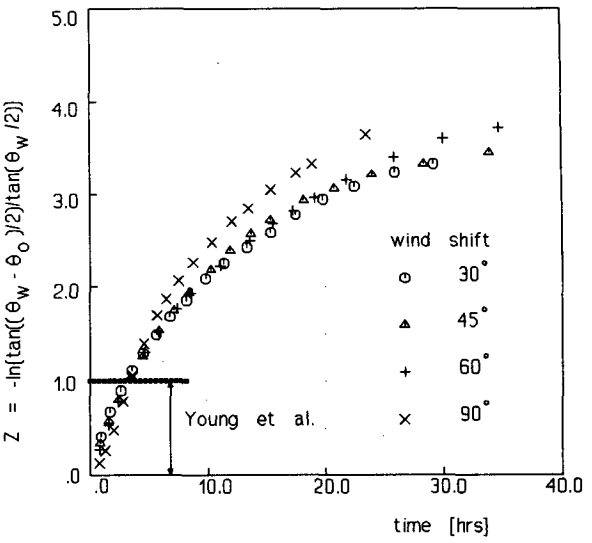

FIG. 4. The response of the mean wave direction to a shift in wind direction in the EXACT-NL wave model (wind speed $U_{10} = 20$ m s^{-1}, various wind shifts). The directional response is transformed such that a constant time scale would give a linear dependency of Z on time. The period of initial response as analyzed by Young et al. (1987) is indicated.

To remedy this, we smooth these time series with a triangular convolution filter, the base interval of which is equal to three time steps on either side of the data point considered. This definition in terms of time step Δt ensures that the filter dynamically adjusts to the instantaneous growth rate of the wave field because the time step in the EXACT-NL model is dynamically adjusted to this (Van Vledder and Weber 1988). This also implies that the width of the filter remains small compared with the time scale of turning [it being roughly proportional to the time scale of energy growth (Holthuijsen et al. 1987)]. The choice of a filter width of three time steps on either side was made on the basis of experiments with the sudden wind-shift case, which has been described above (wind shift = 60° and wind speed $U_{10} = 20$ m s^{-1}). These experiments show that the scatter in τ_* as a function of wave age ν_* is sharply reduced between filter widths of one and three time steps on either side (see Fig. 5 where the filter widths are indicated as Δt, $3\Delta t$, and $5\Delta t$).

To estimate the time scale in the case of the constantly rotating wind, we use the analytical solution of the relaxation model for the stationary situation

$$\tau = \frac{1}{\Omega}\sin(\delta\theta). \qquad (20)$$

These estimated time scales quantify the net result of the processes of generation and dissipation involved. To assess the relative importance of each of these processes individually, we formulate the contribution of these processes in terms of constituent time scales. These are defined as follows. The time scale τ of the

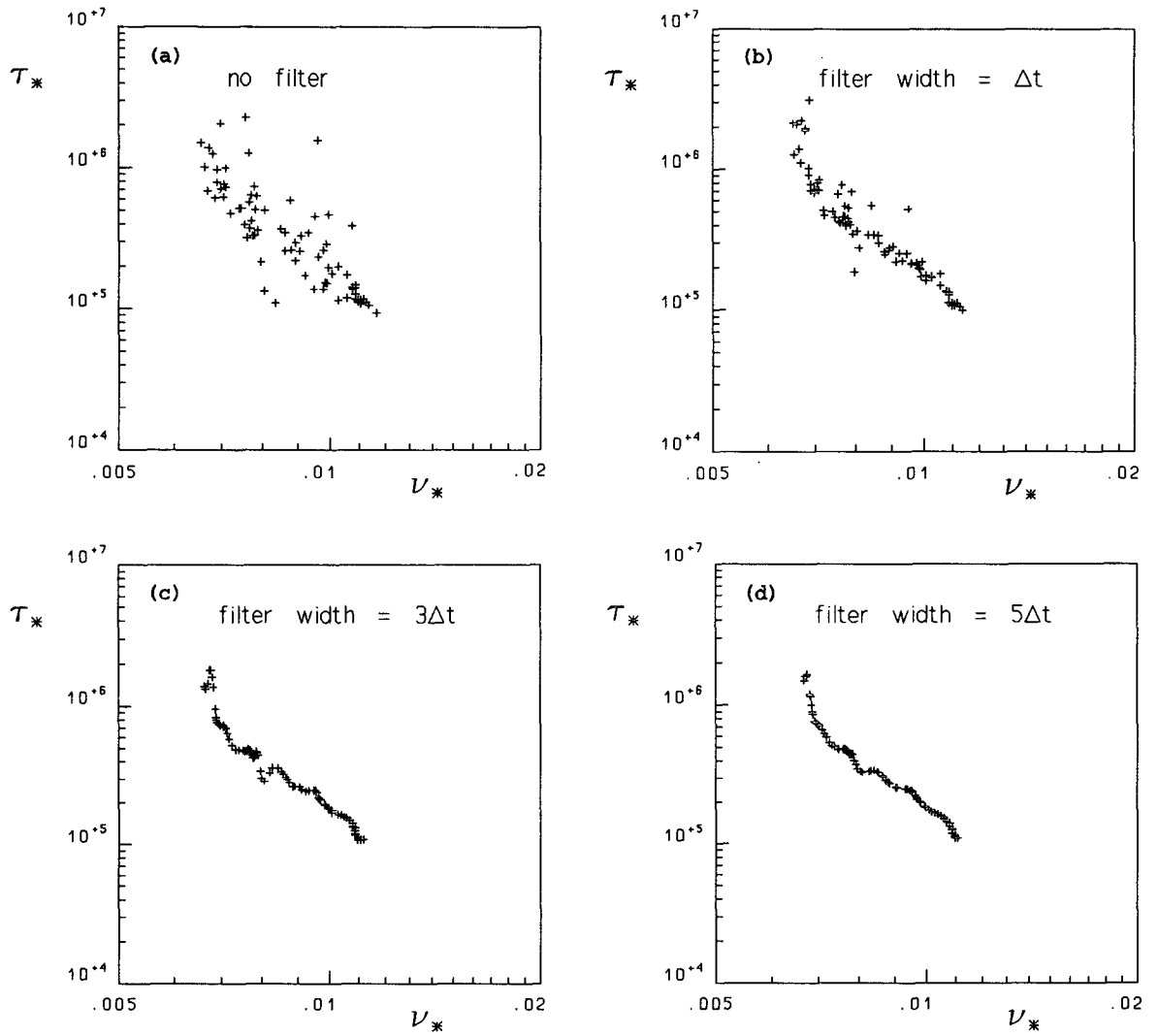

FIG. 5. The effect on the dimensionless response time scale (τ_*) of smoothing the EXACT-NL time series of the mean wave direction with a convolution filter with (one-sided) filter widths Δt, $3\Delta t$, and $5\Delta t$ (the value of Δt adjusts dynamically during the computations). The wind shift is 60°, and the wind speed U_{10} = 20 m s^{-1}. The filter width of $3\Delta t$ has been adopted.

frequency-independent relaxation model is related to the total source function $\partial E(f, \theta)/\partial t = S(f, \theta)$ and the energy spectrum $E(f, \theta)$ as [Holthuijsen et al. (1987) but taking the absolute value of the right-hand side to avoid negative time scales]

$$\frac{1}{\tau} = \left| \frac{\cos(\theta_0) \int_0^{2\pi} \int_0^{\infty} \cos(\theta) S(f, \theta) df d\theta}{\cos(\theta_s) \int_0^{2\pi} \int_0^{\infty} \cos(\theta) E(f, \theta) df d\theta} \right|, \quad (21)$$

where θ_s is the mean direction of the total source term S defined analogously to the mean wave direction θ_0 [with $E(f, \theta)$ replaced by $S(f, \theta)$ in Eq. (3)]. If the source term S is written in its constituent parts S_{in}, S_{ds}, and S_{nl} [Eq. (14)], it is readily shown that the response time scale τ is composed of three time scales corresponding to the atmospheric input (τ_{in}), the whitecapping dissipation (τ_{ds}), and the nonlinear interactions (τ_{nl}). These time scales are defined as τ in Eq. (21), with S replaced by S_{in}, S_{ds}, and S_{nl}, respectively. It can readily be shown that they are related to the total response time scale as

$$\frac{1}{\tau} = \pm \frac{1}{\tau_{in}} \pm \frac{1}{\tau_{ds}} \pm \frac{1}{\tau_{nl}}, \quad (22)$$

the sign in the addition depending on whether the process supports the relaxation toward the wind direction (+) or counteracts it (−). The constituent time scales are interpreted as the contributions of the atmospheric input, the whitecapping, and the nonlinear wave–wave interactions, respectively, to the total time scale.

d. Model results

1) SUDDEN SHIFT

The computed time evolutions of the mean wave direction θ_0, directional width σ_θ, normalized total energy $\epsilon_* (= g^2 E_{tot}/U^4)$, and normalized peak frequency ν_* for the constant wind cases with 20 m s^{-1} are given in Fig. 6.

The response of the mean wave direction θ_0 (Fig. 6a) at first glance seems to be fairly consistent with the behavior of a relaxation model with constant time scale, but we have shown in Fig. 4 that this is only approximately true. The directional width σ_θ of the spectrum [standard deviation of the frequency-integrated directional energy distribution (Kuik et al. 1988)] initially widens and then returns to its original value (Fig. 6b). This behavior has been observed earlier by Kuik and Holthuijsen (1981) in open-sea conditions. Masson (1990) concluded from similar observations that the magnitude of the widening depends on the rate of turning of the wind. In the present model results it is correspondingly more pronounced for the larger directional shifts than for the smaller ones. Figure 6c shows that for the larger wind shifts the net growth of the normalized wave energy ϵ_* stagnates initially. Figure 6d shows that the variation in wave age ν_* is considerable (any dependency on wave age can therefore not be ignored during the turning event).

The evolutions of the two-dimensional spectrum for the smallest wind shift ($\Delta\theta_w = 30°$) and the largest wind shift ($\Delta\theta_w = 90°$) are given in Fig. 7. We show only the results for the cases with $U_{10} = 20$ m s^{-1}, as they are very similar to those for $U_{10} = 10$ m s^{-1}. This shows that initially in both situations a secondary peak is generated near the new wind direction. As this new peak is generated at the high frequencies it is evident that the mean direction at the higher frequencies responds quicker than at the lower frequencies. In the 30° shift case, the rapid merging of the new peak with the old peak gives the impression of the entire spectrum slowly rotating [as noted earlier by Young et al. (1987)]. In the case of the 90° shift the two peaks remain discernable until the original peak has disappeared.

The physical processes involved are presented in Fig. 8, with the individual source functions at a moment in time roughly half-way through the complete directional turn in these two cases. In both cases the atmospheric input (S_{in}) generates high-frequency energy between the new and the old wind direction. (Its mean direction, not shown here, is located between these directions.) In the 30°-shift case, however, the wind still supports the old spectrum (atmospheric input around the old spectral peak), whereas in the 90°-shift case the old spectrum is no longer supported (no atmospheric input around the old spectral peak). The pos-

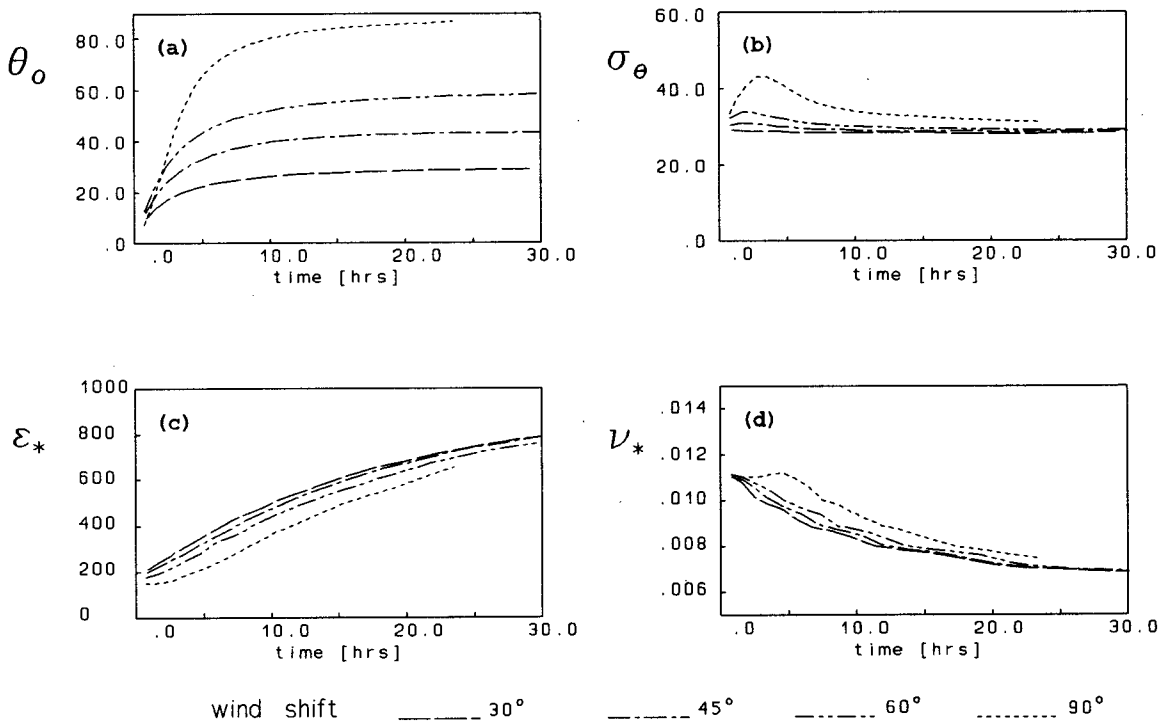

FIG. 6. The response in the EXACT-NL model of the mean wave direction (θ_0), the directional width (σ_θ), the dimensionless wave energy (ϵ_*), and the dimensionless peak frequency (wave age, ν_*) to a shift in wind direction (wind speed $U_{10} = 20$ m s^{-1}, various wind shifts).

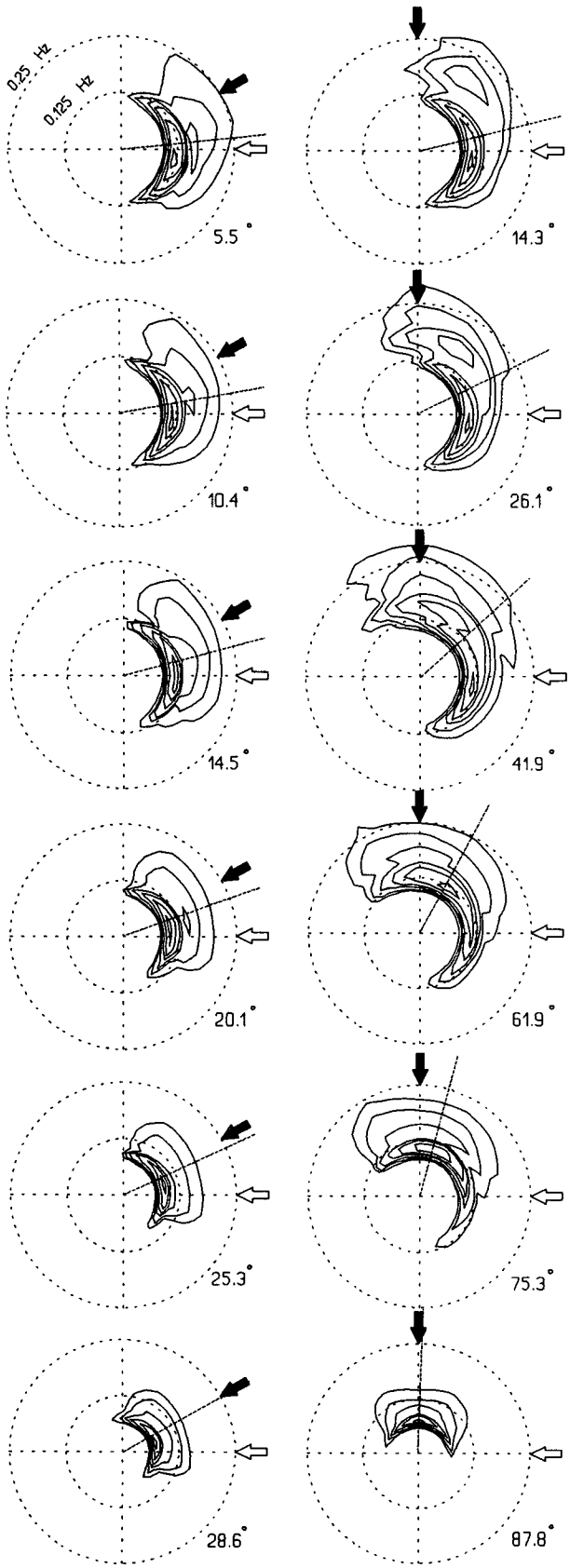

FIG. 7. Evolution of the wave spectrum [$E(f, \theta)$] in the EXACT-NL model for wind shifts of 30° and 90°, and wind speed U_{10} = 20 m s^{-1}. Logarithmic contour intervals of the spectral density (normalized with the peak density, starting at 0.8, interval is a factor 2). Blank arrows indicate the old wind direction; solid arrows indicate the new wind direction. The line radiating from the origin of the spectral plane indicates the mean wave direction, which is also given numerically.

itive and the negative part of the nonlinear interactions (S_{nl}^{+} and S_{nl}^{-}, respectively) are located in the spectral plane such that the newly generated energy is transported from the new wind direction toward the old spectral peak. This implies that the interactions hinder the turning of the waves, even though they conserve energy. The whitecapping source function (S_{ds}) is biased toward the new wind direction. It therefore removes more energy from the new direction than from the old direction, thus opposing the turning of the mean wave direction. Quantitatively the effects of the three different processes are given with the time scales τ_{in}, τ_{ds}, and τ_{nl} in Fig. 9 for all cases with U_{10} = 20 m s^{-1}. It is obvious that the processes are most active immediately after the shift in wind direction and that the atmospheric input (necessarily) dominates the turning of the spectrum. Whitecapping is obviously a strong counteracting process; its time scale being roughly 50% of that for the atmospheric input (but of opposite sign). The contribution of the nonlinear interactions is small.

2) ROTATING WIND

The result for the rotating wind case is a directional lag of $\delta\theta$ = 60.2° with a peak frequency f_{peak} = 0.188 Hz, a total variance of E_{tot} = 0.141 m^2, and a directional width σ_θ = 57.8°. An inspection of the source functions in the stationary situation (not shown here) indicates that the tendencies of the processes are the same as in the constant wind cases. The mean direction of the atmospheric input is lagging behind the wind direction; the nonlinear interactions are supporting the lagging spectral peak; and the whitecapping is biased toward the wind direction.

As indicated in the Introduction, it has been suggested in the literature that the time scale of the directional response is dependent on wave age. For all cases (wind shift 30°, 45°, 60°, and 90°; U_{10} = 10 and 20 m s^{-1}; and the rotating-wind case) the time scales have been plotted in dimensionless form (τ_*) as a function of wave age (ν_*) in Fig. 10. It is obvious that the model time scales increase as the waves develop (ν_* becoming smaller). A least-squares fit through these results (for $\nu_* > 0.007$ to avoid the transition to the fully developed state) gives the following analytical relationship:

$$\tau_* = 0.002\nu_*^{-4.0}. \quad (23)$$

The average χ value for these model results is 0.16 $\times$ 10^{-2} [obtained from each τ_*-value and C_d from

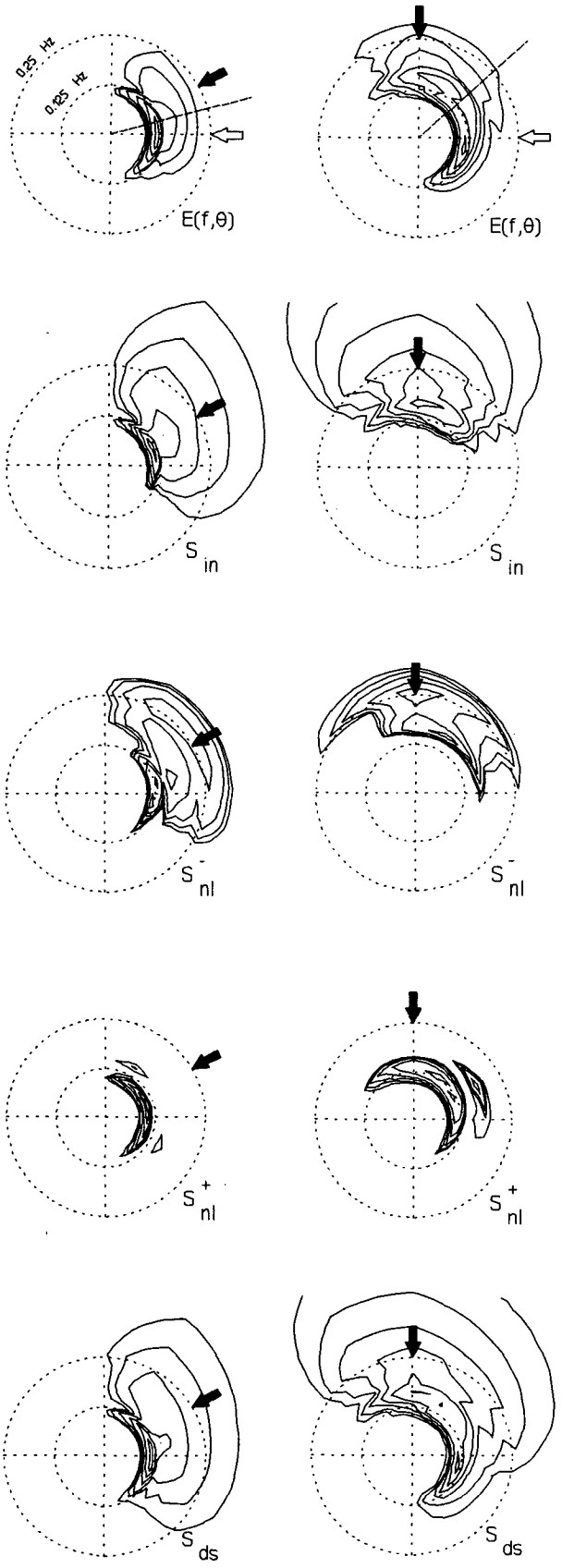

(1); see Table 3], but the preceding best-fit does not support the power of ν_* in the expression defining χ (11) so that the use of this χ value is practically meaningless.

e. *Comparison with published model results*

As indicated earlier, Young et al. (1987) also carried out computations with the EXACT-NL model to evaluate the directional response of waves. They estimated the time scales from a least-squares fit of $Z = -\ln\{\tan(\frac{1}{2}[\theta_w - \theta_0])/\tan(\frac{1}{2}\theta_w)\}$ as a function of time [but only for the initial response; that is, $Z < 1.0$ (I. R. Young, personal communication 1987, see Fig. 4)]. To transform the results of Young et al. (1987; see Table 3) from a frequency-dependent time scale to a frequency-independent time scale, we used the same technique as for the observations of Hasselmann et al. (1980), Allender et al. (1983), and Masson (1990). The result is shown in Fig. 11 for the range of wave age considered by Young et al. (1987).

Another, entirely different model approach has been taken by Günther et al. (1981) and Holthuijsen et al. (1987), who parameterized the energy balance equation. Günther et al. (1981) obtained Eq. (11) and used wave directional observations to estimate the value of χ (see Table 3). From a different parameterization of the energy balance, Holthuijsen et al. (1987) obtained estimates of $\tilde{\tau}$, which does not require directional observations. The corresponding $\tau_* - \nu_*$ relationship in Fig. 11 is based on Eqs. (17) and (18) of Holthuijsen et al. (1987), the relationship for wind seas of Hasselmann et al. (1976, their table 1: $\epsilon = 7.4 \times 10^{-6} \nu^{-3.05}$), and the value of C_d as before ($C_d = 0.001736$).

It is obvious from Fig. 11 that our results for more developed sea states supplement those of Young et al. (1987) at younger sea states. The model of Holthuijsen et al. (1987) apparently predicts time scales similar to those of the EXACT-NL model, except for mature sea states where it predicts smaller time scales. This is due to the fact that in the EXACT-NL model the fully developed stage, where $\tilde{\tau} \to \infty$, is reached at higher values of ν_* than according to Pierson–Moskowitz (1964) used in the model of Holthuijsen et al. (1987).

4. Discussion and conclusions

Our results with the EXACT-NL model indicate that the locally induced turning of waves, which of course is dominated by atmospheric input, is counteracted by whitecapping and nonlinear wave–wave interactions that siphon energy away from the new wave system,

FIG. 8. The wave spectrum [$E(f, \theta)$] in the EXACT-NL model halfway during the turning events of Fig. 7 (θ_0 = 14.5 and 41.9°, respectively) and the corresponding source functions for atmospheric input (S_{in}), nonlinear wave–wave interactions (negative part, S_{nl}^- and positive part, S_{nl}^+), and whitecapping dissipation (S_{ds}). For directional orientation see Fig. 7.

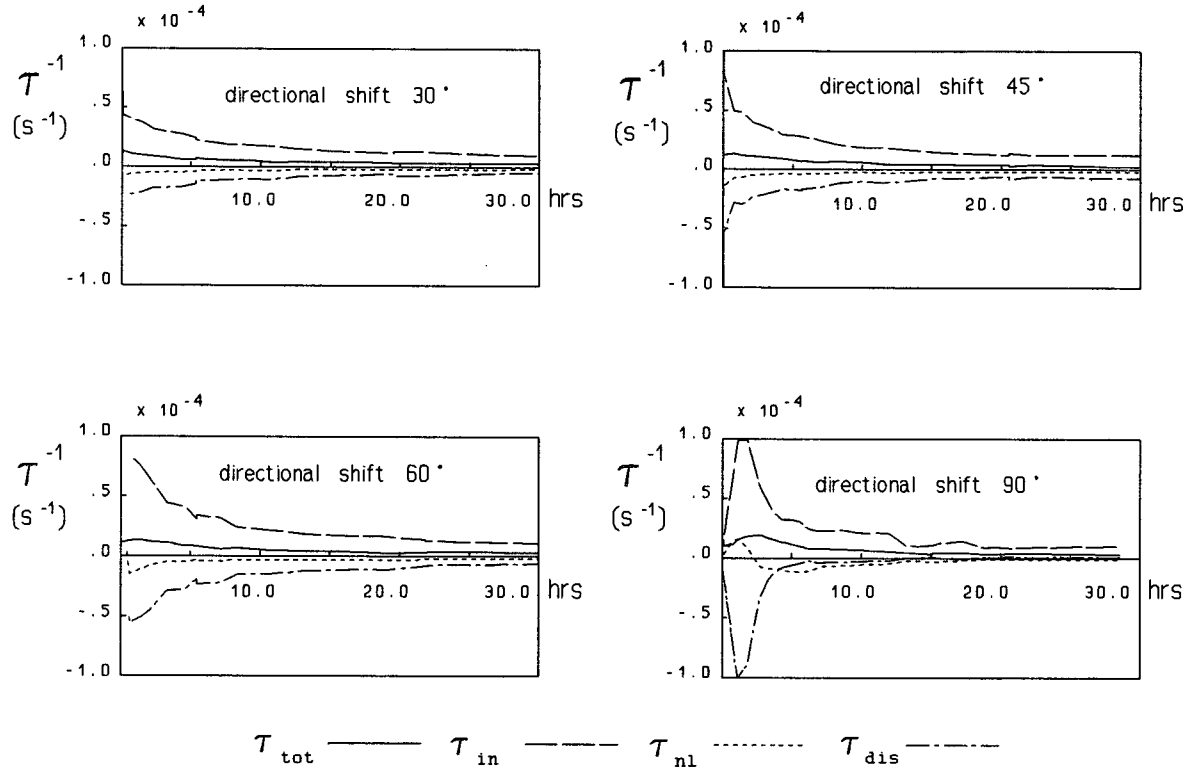

FIG. 9. The (inverse) response time scale (τ^{-1}) in the EXACT-NL model as a function of time and various wind shifts (wind speed U_{10} = 20 m s^{-1}) and its constituent (inverse) time scales due to atmospheric input (τ_{in}^{-1}), nonlinear wave–wave interactions (τ_{nl}^{-1}), and whitecapping dissipation (τ_{ds}^{-1}). The sum of the inverse constituent time scale equals the inverse response time scale (τ^{-1}).

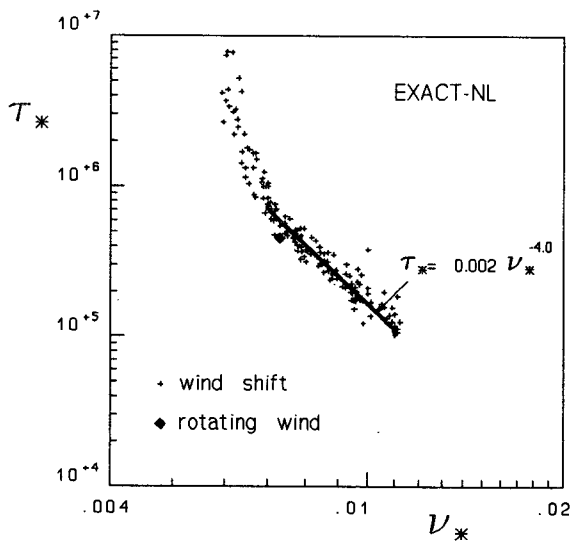

FIG. 10. Dimensionless response time scale (τ_*) in the EXACT-NL model as a function of wave age (ν_*) for all cases considered (wind shifts of 30°, 45°, 60°, and 90°, for wind speed U_{10} = 10 and 20 m s^{-1}, crosses; and constantly rotating wind at 10° h^{-1}, wind speed U_{10} = 20 m s^{-1}, solid diamond). The best-fit approximation for $\nu_* > 0.007$ is indicated.

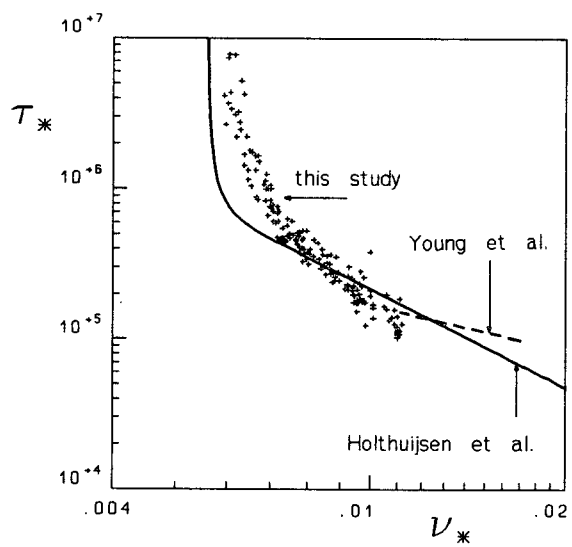

FIG. 11. Dimensionless response time scale (τ_*) in the EXACT-NL model as a function of wave age (ν_*) in the present study compared with the EXACT-NL results of Young et al. (1987) and the model of Holthuijsen et al. (1987). For symbols see Fig. 10.

partly to support the old wave system. From the quantitative analysis of the response we see that atmospheric input alone would turn the mean wave direction very rapidly toward the new wind direction, but this is fairly strongly opposed by whitecapping. The opposition of the nonlinear interactions is minor. We speculate that in general at some moment during a turning event the role of the nonlinear interactions would change from opposing to supporting the turning of the waves. This speculation is based on the fact that in general these interactions support a unimodal spectrum that in a turning-wind event would ultimately be directed in the new wind direction. The nonlinear interactions would therefore shift support from the old (unimodal) spectrum to the new (unimodal) spectrum. In the particular cases studied here, however, the waves were already halfway to being fully developed when the wind shifted and the nonlinear interactions probably faded as the waves achieved the fully developed state. This may not be the case if the waves are younger at the moment of wind shifting. In our numerical experiments the shape of the spectrum is initially (after the wind shift) always bimodal with a secondary spectral peak near the new wind direction. If the wind shift is relatively small (small compared with the directional width of the spectrum), this secondary peak quickly merges with the old peak to form the main peak. The spectrum then seems to rotate as a unimodal shape (as reported by Young et al. 1987). If the wind shift is large, the secondary peak retains its identity and evolves into the main peak as the old wave system decays.

Our observed time scales, which are corrected for the radiative effects of inhomogeneities in the wave field and selected on the basis of geophysical conditions and sampling errors, are generally shorter by a factor of 2 to 3 than our EXACT-NL model time scales, but they converge to the same value at young sea states (Fig. 12). These differences cannot be explained with errors in the observations that are less than 100%. The basic assumption in the parameterization (the dimensionless time scale τ_* is a function of an integral wave age ν_*), however, may be questionable. In fact, in a rapidly turning-wind situation a considerable fraction of the wave energy would not be affected by the wind, and one may want to ignore this fraction in any parameterization. The differences may also be due to errors in the numerical wave model. The most uncertain part of the numerical wave model is the formulation of the whitecapping. It is scaled with two direction-independent wave parameters (total energy and mean frequency, partly joined in a steepness parameter), which implies a strong interaction between wave fields from different directions, irrespective of their direction. This seems to be unrealistic. Within the framework of the present formulation, the dissipation is particularly sensitive to the mean frequency that appears as $\bar{\omega}^7$ in the model. A sensitivity analysis in which the values of the coefficients C, m, and n of (16) were varied as

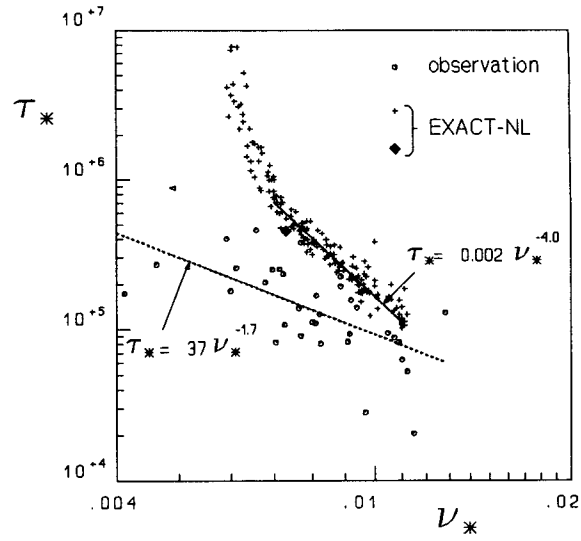

FIG. 12. Dimensionless response time scale (τ_*) as a function of wave age (ν_*) from the observations and from the EXACT-NL model in the present study (for symbols see Figs. 2 and 10). The best-fit approximations are indicated (within the fit range).

in Komen et al. (1984), however, indicated that these realistic changes (and therefore the correspondingly realistic changes in the power of $\bar{\omega}$) cannot account for the differences between the observations and the model results.

The EXACT-NL model does not include a source term for (initial) linear wave growth. This may be important in the 90° wind-shift case, where new wind-wave generation occurs in almost empty regions in spectral space. This lack could artificially slow down the wave-turning process. Computations for the same case with a similar model (namely, the WAM-model, WAMDI, 1988, but with a simpler treatment of the nonlinear interactions), however, have shown that the effect of including a linear growth term in the numerical model is negligible with respect to the turning rate of the mean wave direction.

Acknowledgments. With pleasure we acknowledge the considerable support of a number of people and institutions. We wish to express our special thanks to K. Hasselmann and S. Hasselmann of the Max-Planck-Institute of Meteorology in Hamburg for their generous support and their permission to use the EXACT-NL model. Similarly, we are indebted to P. E. Francis of the United Kingdom Meteorological Office in Bracknell, and J. Guddal and M. Reistad of the Norwegian Meteorological Institute in Bergen for their help and support in the North Sea hindcasts. The Ministry of Public Works and Transport in the Netherlands provided us with the wave observations, and we are particularly grateful to A.J.M. v.d. Vlugt of the Department of Hydro-instrumentation. Permission to use the wind data of Shell Expro U.K. and Pennzoil NedComp

is greatly appreciated. For extended and inspiring discussions we wish to thank I. R. Young of the Australian Defense Force Academy and J. A. Battjes of the Delft University of Technology. The effort of one of the authors (G.Ph. v. Vledder) was sponsored by the Technology Foundation in the Netherlands (STW).

APPENDIX

Effect of Inhomogeneities in the Wave Field on the Local Development of the Mean Wave Direction

The rate of change of the mean wave direction θ_0 due to the effects of local generation and dissipation and due to radiative effects (inhomogeneities in the wave field) can be obtained from the full energy balance equation

$$\frac{\partial E(f,\theta)}{\partial t} + c_g \cdot \nabla E(f,\theta) = S(f,\theta). \quad \text{(A1)}$$

As an intermediate step, we apply the operators that define the mean direction [Eq. (3) of main text] to this equation. The result is

$$\begin{pmatrix} \partial a/\partial t \\ \partial b/\partial t \end{pmatrix}_L + \begin{pmatrix} \partial a/\partial t \\ \partial b/\partial t \end{pmatrix}_R = \begin{pmatrix} \partial a/\partial t \\ \partial b/\partial t \end{pmatrix}_S, \quad \text{(A2)}$$

where

$$\begin{pmatrix} \partial a/\partial t \\ \partial b/\partial t \end{pmatrix}_L = \int_0^{2\pi} \int_0^{\infty} \begin{pmatrix} \cos(\theta) \\ \sin(\theta) \end{pmatrix} \frac{\partial E(f,\theta)}{\partial t} \, df d\theta, \quad \text{(A3)}$$

$$\begin{pmatrix} \partial a/\partial t \\ \partial b/\partial t \end{pmatrix}_R = \int_0^{2\pi} \int_0^{\infty} \begin{pmatrix} \cos(\theta) \\ \sin(\theta) \end{pmatrix} \{ c_g \cdot \nabla E(f,\theta) \} \, df d\theta, \quad \text{(A4)}$$

$$\begin{pmatrix} \partial a/\partial t \\ \partial b/\partial t \end{pmatrix}_S = \int_0^{2\pi} \int_0^{\infty} \begin{pmatrix} \cos(\theta) \\ \sin(\theta) \end{pmatrix} S(f,\theta) \, df d\theta, \quad \text{(A5)}$$

and where the subscripts L, R, and S refer to "local," "radiative," and "source term," respectively.

Since the local rate of change of the cosine and sine of θ_0 (a and b) is estimated from buoy observations, the subscript L will be replaced by *observed*. If these values are known at time t_{j-1}, then the locally induced values of a and b at time t_{j+1} (indicated with *) can be estimated by integrating Eq. (A2) without transport terms and by using a central difference approximation:

$$\begin{pmatrix} a \\ b \end{pmatrix}^*_{j+1} = \begin{pmatrix} a \\ b \end{pmatrix}_{j-1,\text{observed}} + (2\Delta t) \begin{pmatrix} \partial a/\partial t \\ \partial b/\partial t \end{pmatrix}_{j,S}. \quad \text{(A6)}$$

The second term on the right-hand side of Eq. (A6), representing the local effects of generation and dissipation on the values of a and b at time t_{j+1}, can be estimated from a numerical wave hindcast in two ways: either from the theory of wave generation and dissipation, or from the balance between calculated local transport and the observed local rate of change. The second option involves the well-established theory of propagation rather than the less well-established theory of generation and dissipation. For that reason we use the second option. The parameterized source function is then obtained with a central difference scheme:

$$\begin{pmatrix} \partial a/\partial t \\ \partial b/\partial t \end{pmatrix}_{j,S} = \frac{1}{(2\Delta t)} \left\{ \begin{pmatrix} a \\ b \end{pmatrix}_{j+1,\text{observed}} - \begin{pmatrix} a \\ b \end{pmatrix}_{j-1,\text{observed}} \right\} + \begin{pmatrix} \partial a/\partial t \\ \partial b/\partial t \end{pmatrix}_{j,R}, \quad \text{(A7)}$$

in which the radiative term is obtained with a numerical wave hindcast model [with Eq. (A4)]. The subscript R will therefore be replaced by *hindcasted*. Substitution of Eq. (A7) in Eq. (A6) gives the expression that is used in the main text,

$$\begin{pmatrix} a \\ b \end{pmatrix}^*_{j+1} = \begin{pmatrix} a \\ b \end{pmatrix}_{j+1,\text{observed}} + (2\Delta t) \begin{pmatrix} \partial a/\partial t \\ \partial b/\partial t \end{pmatrix}_{j,\text{hindcasted}} \quad \text{(A8)}$$

REFERENCES

Allender, J. H., J. Albrecht, and G. Hamilton, 1983: Observations of directional relaxation of wind sea spectra. *J. Phys. Oceanogr.*, **13**, 1519–1525.

Eide, L. I., M. Reistad, and J. Guddal, 1986: A comparison of hindcast studies with a) a coupled discrete wave model and b) a coupled hybrid wave model. *Proc. Int. Workshop on Wave Hindcasting and Forecasting*, Halifax, Nova Scotia, Environmental Studies Resolving Funds, Report Series No. 065. Ottawa, 153–159.

Greenwood, J. A., V. J. Cardone, and L. M. Lawson, 1985: Intercomparison test version of the SAIL wave model. *Ocean Wave Modelling*, The SWAMP group, Plenum, 256 pp.

Günther, H., W. Rosenthal, and M. Dunckel, 1981: The response of surface gravity waves to changing wind direction. *J. Phys. Oceanogr.*, **10**, 718–728.

Hasselmann, D. E., M. Dunckel, and J. A. Ewing, 1980: Directional wave spectra observed during JONSWAP 1973. *J. Phys. Oceanogr.*, **10**, 1264–1280.

Hasselmann, K., 1960: Grundgleichungen der Seegangsvoraussage. *Schiffstechnik*, **7**, 191–195.

——, 1962: On the non-linear energy transfer in a gravity-wave spectrum. Part 1: General theory. *J. Fluid. Mech.*, **12**, 481–500.

Hasselmann, K., D. B. Ross, P. Müller, and W. Sell, 1976: A parametric wave prediction model. *J. Phys. Oceanogr.*, **6**, 200–228.

Hasselmann, S., and K. Hasselmann, 1981: A symmetrical method of computing the nonlinear transfer in a gravity wave spectrum. *Hamburger Geophys. Einzelschriften*, Reihe A, **Heft 52**, 163 pp.

——, and K. Hasselmann, 1985: The wave model EXACT-NL. *Ocean Wave Modelling*, The SWAMP group, Plenum, 256 pp.

Holthuijsen, L. H., A. J. Kuik, and E. Mosselman, 1987: The response of wave directions to changing wind directions. *J. Phys. Oceanogr.*, **17**, 845–853.

Komen, G. J., S. Hasselmann, and K. Hasselmann, 1984: On the existence of a fully developed wind-sea spectrum. *J. Phys. Oceanogr.*, **14**, 1271–1285.

Kuik, A. J., and L. H. Holthuijsen, 1981: Buoy observation of directional wave parameters. *Proc. Conf. on Directional Wave Spectra Applications*, R. L. Wiegel, Ed., University of California, Berkeley, ASCE, 61–70.

——, G. Ph. van Vledder, and L. H. Holthuijsen, 1988: A method for the routine analysis of pitch-and-roll buoy wave data. *J. Phys. Oceanogr.*, **18,** 1020–1034.

Longuet-Higgins, M. S., D. E. Cartwright, and N. D. Smith, 1963: Observations of the directional spectrum of sea waves using the motions of a floating buoy. *Ocean Wave Spectra,* Prentice Hall, 111–136.

Masson, D., 1990: Observations of the response of sea waves to veering winds. *J. Phys. Oceanogr.*, **20,** 1876–1885.

Mood, A. E., F. A. Graybill, and D. C. Boes, 1974: *Introduction to the Theory of Statistics.* 3d ed. McGraw-Hill, 564 pp.

Pierson, W. J., and L. Moskowitz, 1964: A proposed spectral form for fully developed wind seas based on the similarity theory of S. A. Kitaigorodskii. *J. Geophys. Res.*, **69**(24), 5181–5190.

Riissanen, J., 1975: Some features of wind variation in the friction layer at Helsinki airport. *Finn. Meteor. Inst. Contrib.*, **80,** 40 pp.

Snyder, R. L., F. W. Dobson, J. A. Elliott, and R. B. Long, 1981: Array measurements of atmospheric pressure fluctuations above surface gravity waves. *J. Fluid Mech.*, **102,** 1–59.

Van der Vlugt, A. J. M., 1984: Experiences with the WAVEC buoy. *Proc. Symp. on Description and Modelling of Directional Seas,* Technical University, Denmark, Danish Hydraulic Institute and Danish Maritime Institute, paper A3.

Van Vledder, G. Ph., and S. L. Weber, 1988: Guide for the program EXACT-NL, Max-Planck-Institut für Meteorologie, Hamburg, Rep. No. 20, 27 pp.

Van Vledder, G. Ph., 1990: Directional response of wind waves to turning wind waves. Communications on hydraulic and geotechnical engineering. Doctoral thesis, Delft University of Technology, Fac. of Civil Engineering Report 90-2, 255 pp.

Vermeulen, P. E. J., B. Oemraw, and J. Wieringa, 1985: Wind tunnel measurements of the flow distortion near the anemometer positions on PENNZOIL K13-A platform. Netherlands Organization for Applied and Scientific Research, Fluid Dynamics Department, Apeldoorn, The Netherlands, Rep. No. 85-01246, 16 pp.

WAMDI Group, 1988: The WAM model—A third-generation ocean wave prediction model. *J. Phys. Oceanogr.*, **18,** 1775–1810.

Wu, J., 1982: Wind-stress coefficients over sea surface from breeze to hurricane. *J. Geophys. Res.*, **87**(C12), 9704–9706.

Young, I. R., S. Hasselmann, and K. Hasselmann, 1987: Computations of the response of a wave spectrum to a sudden change in wind direction. *J. Phys. Oceanogr.*, **17,** 1317–1338.